

Artificial magnetic fields in spin chains with long-range interactions - fractal energy spectra and topological phases

Tobias Graß¹, Christine Muschik^{1,2,3}, Alessio Celi¹, Ravindra Chhajlany^{1,4}, Maciej Lewenstein^{1,5},

¹ICFO-Institut de Ciències Fotòniques, Av. Carl Friedrich Gauss 3, 08860 Barcelona, Spain

²Institute for Quantum Optics and Quantum Information of the Austrian Academy of Sciences, A-6020 Innsbruck, Austria

³Institute for Theoretical Physics, University of Innsbruck, A-6020 Innsbruck, Austria

⁴Faculty of Physics, Adam Mickiewicz University, Umultowska 85, 61-614 Poznań, Poland and

⁵ICREA-Institució Catalana de Recerca i Estudis Avançats, Lluís Companys 23, 08010 Barcelona, Spain

Spin chains with tunable interaction range have become available in systems of trapped ions or atoms coupled to waveguides. The spin chain can be mapped onto hard-core bosons moving on a higher-dimensional graph, where the dimensionality of the graph is given by the range of the interactions. We propose to use shaking techniques to mimic magnetic fields. This can lead to a fractal energy spectrum, and the appearance of topological phases, which we reveal by calculating edge states and Chern numbers.

Introduction. When an electric charge moves on a closed loop in the presence of a magnetic field, its wavefunction picks up a geometric phase according to the magnetic flux through the contour. In a discretized, two-dimensional space, the commensurability condition between lattice and flux together with the gapped structure of energy levels give rise to a fractal energy spectrum, known as the Hofstadter butterfly [1]. Apart from its esthetical appeal, the intriguing physics of topological order has triggered immense interest in this phenomenon. In recent years, engineering topological quantum systems with cold atoms in artificial gauge fields has become a major field of research [2–17]. However, since the effect of a magnetic field is trivial in one spatial dimension, as any loop encloses zero flux, promising platforms such as trapped ions [18, 19] or atoms coupled to waveguides [20–23] have been excluded from quantum simulations of the Hofstadter model.

In this work, we open an avenue for implementing topological order in dressed 1D systems. We exploit the long-range character of interactions, and mimic magnetic fluxes through complex interaction parameters. The hopping of a particle is represented by spin flips in an XY spin chain, and a sequence of spin flips which returns to the initial configuration is interpreted a closed loop. A non-zero “magnetic” flux through such loop is obtained if the complex phase of the interaction is not proportional to the distance of the spins. We show that this model supports a butterfly-like fractal energy spectrum, non-zero Chern numbers, and localized edge states, similar to the ones of the Aubry-André model [24–26].

For the implementation of the spatially dependent, complex couplings in 1D systems with long range interactions, we propose a scheme inspired by lattice shaking methods, which were introduced for cold atoms in optical lattices [10, 11, 27–39], and also for ions in 2D microtraps [40]. Our approach allows one to custom-tailor arbitrary interaction strengths and hopping phases. In the following, we focus on a special case that allows for the observation of topologically non-trivial bands and can

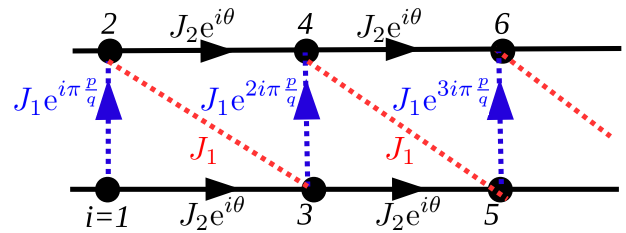


FIG. 1: (Color online) Spin chain with NN bounds (dashed) and NNN bounds (black solid), mapped on a triangular ladder.

be implemented with an overhead that is independent of the number of atoms involved.

Model. We consider an XY spin chain $H = -\sum_{i \neq j} (J_{ij} \sigma_i^+ \sigma_j^- + \text{H.c.}) + h \sum_i \sigma_i^z$, with possibly long-range spin-spin interactions J_{ij} , and a polarizing transverse field h . For $|h| \gg |J_{ij}|$, all spins are aligned in z -direction. Low-lying excitations consist of a single spin flip, that is, they belong to the subspace with total spin $S_z = \sum \sigma_i^z = N - 2$, where N is the total number of spins. In this subspace, the spin-flip interaction of the XY model maps onto a free hopping model of a single particle in a chain. For $|S_z| < N - 2$, a mapping onto a free fermion model can be achieved via a Jordan-Wigner (JW) transformation if interactions are restricted to nearest neighbors. In the presence of long-range interactions, the JW transformation produces also occupation-dependent tunneling terms. More conveniently, the spin model with long-range interactions is interpreted a system of hardcore bosons. We assume complex interaction parameters $J_{ij} = |J_{ij}| \exp(i\varphi_{ij})$, which are associated with minimal coupling to a vector potential.

As described in the Supplemental Material (SM), the effective couplings can be tailored such that one obtains nearest-neighbor (NN) interactions of constant strength J_1 and next-nearest-neighbor (NNN) interactions of con-

stant strength J_2 , while all other interaction terms are negligible. The chain can then be mapped onto a triangular ladder where each site is back- and forward connected to a NNN via the horizontal bounds, as well as to the two NNs via the other bounds, see Fig. 1. More generally, a spin chain with long-range interactions can be mapped onto a graph embedded in larger dimension, defined by the range of the interactions. For instance, including also third-neighbor interactions, the chain can be mapped onto an arrangement of linearly connected tetraheders.

In the following, we focus on the $J_1 - J_2$ model, with $|J_1| = |J_2| = J$, and complex-valued parameters. Viewed as a triangular ladder, the elementary plaquettes are given by three spins $i, i+1$, and $i+2$ forming a triangle. The magnetic flux associated to the i th triangle is $\Phi_i = (-1)^i (\varphi_{i+1,i} + \varphi_{i+2,i+1} + \varphi_{i,i+2})$. Through gauge invariance, the fluxes Φ_i uniquely define the physics. As a convenient choice, we will set phases on NNN links to a constant θ , $\varphi_{i+2,i} = \theta$, while every second NN bond is equipped with a spatially dependent phase: $\varphi_{i+1,i} = \frac{\pi(i+1)p}{2q} \delta_{(i+1) \bmod 2, 0}$, with p and q two coprime integers. With this, the flux through squares in Fig. 1 is $2\pi(p/2q)$.

From a Fourier transform of H , one obtains a Harper-like Hamiltonian [41],

$$H = -J \sum_{k,\nu} \left[e^{ik} (\sigma_{k\nu 1}^+, \sigma_{k\nu 2}^+) \begin{pmatrix} 1 & 1 \\ 0 & 1 \end{pmatrix} \begin{pmatrix} \sigma_{k\nu 1}^- \\ \sigma_{k\nu 2}^- \end{pmatrix} + \right. \\ \left. (\sigma_{k\nu 1}^+, \sigma_{k\nu 2}^+) \begin{pmatrix} 0 & 0 \\ 1 & 0 \end{pmatrix} \begin{pmatrix} \sigma_{k(\nu+1)1}^- \\ \sigma_{k(\nu+1)2}^- \end{pmatrix} \right] + \text{H.c.}, \quad (1)$$

where $\sigma_{k\nu\ell}^\pm$ denote the Fourier-transformed spin-flip operators acting on odd ($\ell = 1$) and even sites ($\ell = 2$). There are $2q$ bands, denoted by ν , with wave vectors k restricted to the magnetic Brillouin zone $[-\pi/2q, \pi/2q]$. All bands are gapped except for the two bands around $E = 0$ which touch each other for even q .

Plotting the energy spectrum versus the flux, one finds a fractal figure shown in Fig. 2(d) for a system of $N = 100$ spins. In view of the different dimensionality, the similarity of this spectrum to the Hofstadter butterfly [1] is surprising. It is seen that this moderate size is sufficient to reveal the fractal nature of the spectrum in the Hilbert space with one spin flip. In contrast, less structure is recognized in the spectrum for $S_z = N - 4$, also shown in Fig. 2(d). Since the energy levels from the $S_z = N - 4$ sector cover almost entirely the gaps of the butterfly, levels with different magnetization have to be distinguished in order to reveal the butterfly structure experimentally. This is possible, for instance, by a sufficiently strong energy shift via the transverse field h . We note that, due to interactions, the energies at $S_z = N - 4$ are not simply the sum of the energies at $S_z = N - 2$.

Topological order. The appearance of a butterfly spec-

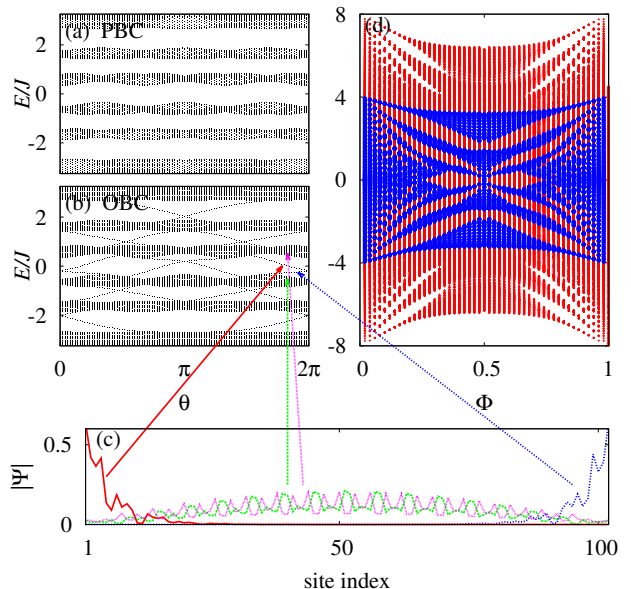


FIG. 2: (Color online) (a,b) Energy spectra (for $S_z = N - 2$) as a function of a constant NNN phase $\varphi_{i,i+2} = \theta$. We consider a system of $N = 102$ spins with a flux $p/q = 1/3$. In (a), we assume periodic boundary conditions, while in (b) the boundary is open. In the latter case, edge states close the gaps. They are localized at the ends of the chain, as seen from the wave function amplitude for selected states plotted in (c). In (d), the energy spectrum with periodic boundary is plotted as a function of the fluxes p/q , for $S_z = N - 2$ (blue) and $S_z = N - 4$ (red) in a system of $N = 100$ spins for $\theta = 0$.

trum is intimately related to quantum Hall physics, where bulk gaps are closed by conducting edge states. To visualize edge states in the single-particle spectrum ($S_z = N - 2$), we consider the energy levels' dependence on the constant NNN phase θ for open and periodic boundary conditions, see Fig. 2(a-b). With q being odd, all energy bands are gapped for any θ in the periodic system, but with an open boundary, one finds edge states connecting the bands. As seen in Fig. 2(c), the edge states in our 1D system localize at the ends of the spin chain, similar to Majorana fermions or to the edge states seen in the Aubry-André model [24].

Another measure of topological order are Chern numbers associated with the energy bands [42]. Chern numbers are robust in the sense that only a perturbation which closes the energy gap can modify their integer value. Their definition requires two parameters on which the Hamiltonian periodically depends. In the case of a single spin-flip, these parameters are given by the wavevector k and the phase θ . The dependence of the eigenstates $|u(k, \theta)\rangle$ on these parameters is measured by the Berry connection, a two-component vector field defined as $A_\mu(k, \theta) = \langle u(k, \theta) | \partial_\mu | u(k, \theta) \rangle$, where $\mu = \{k, \theta\}$. The Chern number is then obtained as the inte-

q	Chern numbers
3	-1, -1, 2, 2, -1, -1
4	-1, -1, -1, 6, -1, -1, -1
5	-1, -1, -1, -1, 4, 4, -1, -1, -1, -1

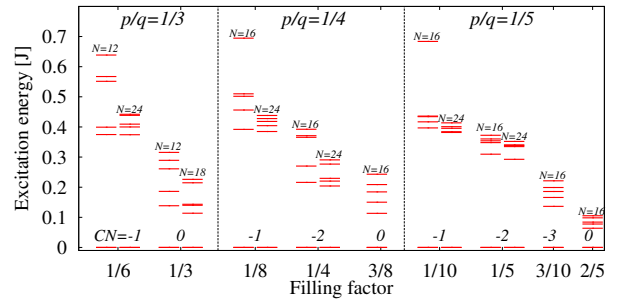
TABLE I: Chern numbers of gapped manifolds at different q .

gral of the Berry curvature over the full parameter space. For those energy bands which form quasidegenerate doublets, we have to consider the non-Abelian Berry connection, $\mathcal{A}_\mu^{rs}(k, \theta) = \langle u_r(k, \theta) | \partial_\mu | u_s(k, \theta) \rangle$, where each component is a $N_{\text{deg}} \times N_{\text{deg}}$ matrix, obtained from the N_{deg} quasidegenerate bands $|u_r(k, \theta)\rangle$, $r = 1, \dots, N_{\text{deg}}$. For calculating the Chern numbers, we follow the method established in Ref. [43] using a discretized set of parameters. As an example, we have listed the results for $p = 1$ and $q = 3, 4, 5$ in Table I.

Our analysis so far has demonstrated that the energy bands at $S_z = N - 2$ are topological, but we still cannot conclude that the system is in a topological insulator phase. The latter would correspond to one or several completely filled bands, e.g. $S_z/N = 1 - 2\nu$, with the filling factor $\nu = 1/q$. In contrast to this, the system at $S_z = N - 2$ corresponds to a single particle, whereas in the presence of several spin flips, for $|S_z| < N - 2$, the XY model maps onto a model of interacting particles. We thus have to investigate to which extent interactions modify the spectrum.

By exact diagonalization, we have studied the many-body scenario with filling factors $\nu = p/(2q)$ for $2 \leq q \leq 5$ and system sizes up to $N = 30$. We can associate a Chern number to the many-body states, by varying the NNN phase θ , and using the twist angle of twisted boundary conditions as a second parameter [44]. While the ground state Chern number at $q = 2$ is always zero, non-zero Chern numbers are found for $q \geq 3$ at sufficiently small p . As shown in Fig. 3, the gap above those topological many-body ground states appears to be robust against increasing the system size. Notably, all non-zero Chern numbers are $-p$, in full agreement with the previous single-particle calculation, see Table I. This indicates that at those ν , despite the interactions, the single-particle picture remains valid. We note that by spin inversion symmetry the same is true for the filling factors $1 - p/q$. On the other hand, no topological order survives close to half-filling: From Fig. 3 we see that the ground state gap becomes smaller (and may vanish for larger systems), and the corresponding Chern numbers are zero. The latter observation excludes fractional Chern insulator behavior for which the gap might be smeared out through topological quasi-degeneracies.

Experimental implementation. Spin chains with tunable long-range interactions are available in systems of trapped ions [18, 19] or using atoms coupled to nanophotonic systems [20, 21]. In the following, we assume inter-

FIG. 3: Energies of the five lowest eigenstates for the XY spin chain with N spins at different filling factors and for different fluxes $2\pi p/q$. The numbers above the ground state denote the many-body Chern number.

actions of the type $\bar{H}_1 = -\sum_{i,j} \bar{J}_{ij} (\sigma_i^+ \sigma_j^- + \sigma_i^- \sigma_j^+) + h \sum_i \sigma_i^z$, and describe a protocol, which allows for the generation of the desired artificial magnetic fields by periodically driving the system (shaking).

Shaking protocols are based on adding fast local terms to the interactions of a system. In our case, they take the form of local energy offsets $\bar{H}_0 = \sum_i v_i(t) \sigma_i^z$, $\bar{H} = \bar{H}_1 + \bar{H}_0$. By performing a gauge transformation $H = U^\dagger \bar{H} U - iU^\dagger \dot{U}$ using $U = e^{-i \sum_i \chi_i(t) \sigma_i^z}$ with $\chi_i(t) = \int_0^t dt' v_i(t')$, one obtains the Hamiltonian $H = -\sum_{ij} (J_{ij} \sigma_i^+ \sigma_j^- + \text{H.c.})$. Note the presence of J_{ij} terms which reduce to a constant for fixed S_z . As the value of the constant depends on the magnetic flux, these terms will distort the butterfly spectrum, but the spectrum can easily be purged. Provided the functions $v_i(t)$ vary on a time scale T^{-1} which is fast compared to the bare dynamics of the system, the evolution of the atoms can be well described using the time averaged effective couplings [27]

$$J_{ij} = \frac{\bar{J}_{ij}}{T} \int_0^T dt e^{2i[\chi_i(t) - \chi_j(t)]}. \quad (2)$$

As explained in detail in the SM, our protocol consists of a sequence of step functions $v_i(t)$ (see Fig. 4a) where the phases $\varphi_{ij} = \arg(J_{ij})$ are encoded in the times at which the energy-offsets of the atoms change. To this end, we define elementary time windows of length Δ and assign frequencies ν_i to the atoms, which are multiples of the basic frequency $\nu_0 = \frac{\pi}{\Delta}$. Two atoms with different frequencies $\nu_i \neq \nu_j$ do not accumulate a contribution to the effective coupling J_{ij} over a time period which is a multiple of the basic time window Δ , since $\int_t^{t+\Delta} e^{i2(\nu_i - \nu_j)t'} dt' = 0$ for $l \in \mathbb{N}$. A non-trivial phase is obtained by choosing the interval $[t_A, t_A + \tau_{ij}]$ in Fig. 4a,b such that τ_{ij} is not a multiple of Δ . With two atoms i and j remaining at different energies ν_i and ν_j during the time interval τ_{ij} , the phase $\varphi_{ij} = 2(\nu_i - \nu_j)\tau_{ij}$ is obtained. In the subsequent interval $[t_A + \tau_{ij}, t_A + \tau_{ij} + m\Delta]$, the energy offsets of two atoms are set to equal values.

v_i	time intervals (in units of Δ)
0	$\left[(i+1) \bmod 2 \cdot (n+1) + \frac{\theta}{4\nu_0\Delta}, \{(i+1) \bmod 2 + 1\} (n+1) + \frac{\theta}{4\nu_0\Delta} \right]$
0	$[2(n+1) + m \cdot H(i \bmod 4 - 1.5), 2(n+1) + m \cdot H(i \bmod 4 - 1.5) + m]$
0	$[2(n+m+1) + (m+1) \cdot H((i-1) \bmod 4 - 1.5) + \frac{t_i}{\Delta}, 2n+3m+3 + (m+1) \cdot H((i-1) \bmod 4 - 1.5) + \frac{t_i}{\Delta}]$
$-i\nu_0$	$[2(n+2m+2), 3(n+2m+2)]$
$i\nu_0$	elsewhere

TABLE II: Shaking functions $v_i(t)$ for realising the interactions shown in Fig. 1. $H(t)$ is the Heaviside function, $\nu_i = i \bmod 4 + 4\delta_{i \bmod 4, 0}$ and $t_i = i \bmod 2 \cdot \frac{\varphi_{i,i+1}}{2\nu_0} + (i+1) \bmod 2 \cdot \frac{\varphi_{i-1,i}}{2\nu_0}$. The angles φ_{ij} take values between 0 and 2π .

Only this interval contributes to the effective coupling strength $|J_{ij}|$, determined by the duration $m\Delta$. Finally, the energy offsets resume their original values $\nu_i \neq \nu_j$ for a time window of length $\Delta - \tau_{ij}$. The contributions that are accumulated during the first and third time window cancel such that $\int_{t_A}^{t_B} e^{i2(\chi_i(t') - \chi_j(t'))} dt' = m\Delta e^{i\varphi_{ij}}$.

The protocol consists of a series of blocks of the type shown in Fig. 4a,b. The whole sequence of length T is repeated periodically. This way, arbitrary couplings can be engineered. The scheme for realizing the specific setting in Fig. 1a is shown in Fig. 4c. The energy offsets take here the values $\nu_0, 2\nu_0, 3\nu_0, 4\nu_0, \nu_0, 2\nu_0, \dots$ along the chain and we assume exponentially decaying couplings \bar{J}_{ij} , as can be realised for atoms coupled to nanophotonic crystals [20, 21]. In this protocol, the energy offset of many atoms is set to zero simultaneously. During time interval I in Fig. 4c, a sequence of the type shown in Fig. 4a,b, is performed for all atoms with odd index (see Table II), such that a contribution to J_{ij} is accumulated for all atoms pairs (i, j) with $i, j = 1 \bmod 2$. However, due to the exponential suppression of the coupling with the interatomic distance, undesired contributions with $|i - j| > 2$ are suppressed. Similarly, the NNN couplings for atoms with even index are determined time interval II. The NN couplings are engineered in the following four sections. Part III and IV correspond to the diagonal links in Fig. 1 and involve atoms with index $i \bmod 4 = 0, 1$ and $i \bmod 4 = 2, 3$ respectively. The phases on vertical links are determined in section V (for $i \bmod 4 = 1, 2$) and in section VI (for $i \bmod 4 = 3, 4$). In section VII, the energy offsets take negative values in order guarantee that $\frac{1}{T} \int_0^T dt v_i(t) = 0$. The general expression for the protocol is given in Table II.

The realization of the scheme requires a well defined separation of the energy scales involved. For the validity of the time averaged description, we require $T^{-1} \gg \bar{J}_{ij}, h$ and the effective coupling rates need to be large compared to the coherence time, $J_{ij} \gg t_{\text{dec}}^{-1}$. Moreover, $h \gg J$ guarantees a separation of the spectra for different magnetisations S_z . Apart from these general consideration, there are constraints which depend on the specific sys-

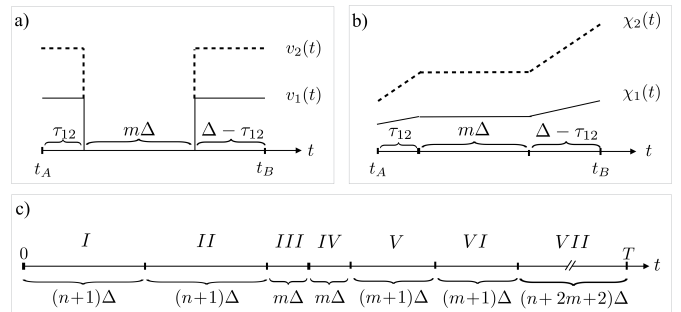


FIG. 4: (a) Time-dependence of the local energy offsets v_i on sites 1 and 2. (b) Plot of the integrated energy offsets χ_i which give rise to complex hopping parameters, see Eq. (2). The resulting phases are given by $\varphi_{ij} = 2\max(v_i - v_j)\tau_{ij}$. As depicted in (c) and explained in the main text, the whole shaking period T is divided into several parts, adjusting the effective strengths $\frac{J_2}{J_1} = \frac{n}{m} \cdot \frac{\bar{J}_2}{\bar{J}_1}$ and the phases of J_{ij} for different pairs.

tem, for example adiabaticity conditions, if the spin-spin interaction is mediated via photons or phonons. In the SM, we discuss a possible implementation using atoms coupled to nanophotonic crystals [20, 21].

Summary and Outlook. In summary, we have shown that a spin chain with long-range and complex-valued interactions shows similar physics as the Hofstadter model for a charged particle in a plane with perpendicular magnetic field. The single-particle system exhibits edge states and a band structure with non-zero Chern numbers. Despite the model's interactions, at different filling factors the many-body ground state corresponds to filled bands. The spin chain is then equivalent to an integer quantum Hall system or a topological insulator.

Our model can be engineered in systems of trapped ions or atoms in waveguides. We provide a protocol to engineer the artificial magnetic field. The high degree of controllability in these systems makes feasible the detection of the fractal energy spectrum or of edge states.

Our analysis is related also to spin chains with Dzyaloshinskii-Moriya interactions [45–47], possibly with long-range character [48]. It holds also for zig-zag ladders incorporating the Hofstadter model [49], and is closely connected to the Hofstadter model with long-range hopping [50]. We note that for certain choices of the gauge potential, a fractal energy spectrum identical to the Hofstadter butterfly can be obtained.

We have focused on the case with nearest-neighbor and next-nearest neighbor interactions. In view of the tunability of the interactions, a systematic study of the influence of longer-range interactions could be a relevant extension of our work. Another interesting aspect would be the generalization from the XY model to a Heisenberg model: The $S_z - S_z$ interaction may provide an additional repulsion between the spin flips, which could give rise to fractional Chern insulator behavior.

Acknowledgements. We wish to thank Philipp Hauke for fruitful discussions. We acknowledge support from ERC advanced Grant OSYRIS, EU IP SIQS, EU STREP EQuaM (FP7/2007-2013 Grant No. 323714), FOQUS, and Fundació Cellex. R.W.C. acknowledges a Mobility Plus fellowship from the Polish Ministry of Science and Higher Education and the (Polish) National Science Center Grant No DEC-2011/03/B/ST2/01903.

Supplemental Material

In the following, we provide details on the generation of artificial gauge fields for the setup under consideration. In Sec. , we explain the protocol for engineering the fluxes shown in Fig. 1 in the main text. In Sec. , we discuss the implementation of this scheme using neutral atoms coupled to photonics crystals [20, 21]. Throughout the Supplemental Material, $\hbar = 1$ will be used.

Engineering artificial gauge fields in 1D spin chains

We consider a chain of regularly spaced atoms with internal levels $|g\rangle$ and $|s\rangle$ that interact according to

$$\bar{H}_1 = - \sum_{i,j} \bar{J}_{ij} (\sigma_i^+ \sigma_j^- + \sigma_j^+ \sigma_i^-) + h \sum_i \sigma_i^z, \quad (3)$$

where $\sigma^+ = |s\rangle\langle g|$, $\sigma^- = |g\rangle\langle s|$ and $\sigma^z = |s\rangle\langle s| - |g\rangle\langle g|$. The interaction strength \bar{J}_{ij} is assumed to decay fast with the distance of the atoms i and j . The shaking recipe put forward here is designed such that a model can be implemented, where the effective nearest neighbour (NN) interactions J_1 and next-to-nearest neighbour (NNN) interactions J_2 are of equal strength while longer-range interactions are negligible. In this case, the 1D-chain can be mapped to a 2D ladder configuration as shown in Fig. 1 in the main text. Apart from equalizing the strength of the NN and NNN interactions, the shaking recipe generates the phases and corresponding nontrivial fluxes shown in Fig. 1 in the main text that are analysed there. With small modifications, the scheme allows one to engineer arbitrary effective couplings J_{ij} with a range that is restricted to NNN interactions. The scaling of the required time resolution and necessary shaking frequencies is hereby independent of the system size.

Shaking

For engineering the effective couplings, we adopt lattice shaking methods (see for example [10, 11, 27]) that are based on adding fast local terms to the bare interaction, $\bar{H} = \bar{H}_1 + \bar{H}_0$. In our case, the shaking Hamiltonian \bar{H}_0 takes the form of a sum of local energy offsets,

$$\bar{H}_0 = \sum_i v_i(t) \sigma_i^z$$

with periodic shaking functions $v_i(t+T) = v_i(t)$. The time dependent canonical transformation

$$U = e^{-i \sum_i \chi_i(t) \sigma_i^z}, \quad \chi_i(t) = \int_0^t d\tau v_i(\tau)$$

yields the transformed Hamiltonian $H = U^\dagger \bar{H} U - i U^\dagger \dot{U}$. If the shaking period T is short compared to the time scales of the bare evolution of the system, \bar{J}_{ij}^{-1} , \hbar^{-1} , the dynamics of the system can be well described using the time averaged Hamiltonian

$$H = - \sum_{ij} (J_{ij} \sigma_i^+ \sigma_j^- + \text{H.c.}) + h \sum_i \sigma_i^z, \quad (4)$$

$$J_{ij} = \frac{\bar{J}_{ij}}{T} \int_0^T dt e^{2i[\chi_i(t) - \chi_j(t)]}. \quad (5)$$

Protocol for engineering the fluxes shown in Fig. 1 in the main text

For the specific shaking protocol proposed here, each shaking function $v_i(t)$ is a steplike function that alternately takes one of the two possible values ν_i or zero as shown in Fig. 4a in the main text (compare also [51]). To this end, we introduce an elementary time window of length Δ , and assign energy offsets ν_i to the atoms that are multiples of $\nu_0 = \frac{\pi}{\Delta}$. We use here $\nu_i = (i \bmod 4 + 4\delta_{i \bmod 4, 0}) \cdot \nu_0$, i.e. energy offsets $\nu_0, 2\nu_0, 3\nu_0, 4\nu_0, \nu_0, 2\nu_0, \dots$ along the chain. This choice ensures that $J_{ij} = 0$ for two atoms that evolve with different energy offsets $\nu_i \neq \nu_j$, since $\int_t^{t+r\Delta} dt' e^{i l \nu_0} = 0$ for $r \in \mathbb{N}$, $l \in \mathbb{N} \setminus \{0\}$. For engineering the coupling J_{ij} , the energy-offsets of the atoms with indices i and j are set to zero during well defined time windows, as explained below. Fig. 5a depicts the shaking cycle for the setting shown in Fig. 1 in the main text. This cycle is repeated periodically and consists of seven time intervals. The time intervals I - VI are used for defining the effective couplings J_{ij} . Time interval I is used to tailor the interactions that correspond to the upper horizontal links in Fig. 1 in the main text. Therefore only atoms with odd indices are addressed. The scheme leads to effective couplings for all atom pairs (i, j) with $i, j = 1 \bmod 2$. Due to the fast decay of \bar{J}_{ij} with the interatomic distance, undesired contributions for $|i - j| > 2$ are suppressed. Time interval II is used to tailor the interactions that correspond to the lower horizontal links in Fig. 1 in the main text and involves therefore only atoms with even indices. The following four sections (III-VI) serve for defining the coupling that are associated with NN interactions. The last time interval in the cycle ensures that the time-average of the shaking function is zero, $\frac{1}{T} \int_0^T dt v_i(t) = 0$. To this end, the energy-offset of each atom takes the constant negative value $-\nu_i$ during time interval VII. The definitions of the shaking functions $v_i(t)$ for a full cycle are given in Table II in the main text.

Basic sequence of the protocol

In each time interval I-VI, the elementary sequence shown in Fig. 4 ab in the main text is performed. The timing of the energy drops in this sequence is crucial both for obtaining the desired phases and for adjusting the interaction strength. Let us assume that the elementary sequence occurs within a time interval $[t_A, t_B]$ with $t_A = 0 \bmod \Delta$ and $t_B = t_A + (n+1)\Delta$ with $n \in \mathbb{N}$. For this time interval, the shaking functions of two atoms with indices i, j and $\nu_i \neq \nu_j$ are given by $v_{i/j}(t) = \nu_{i/j} (1 - H(t - [t_A + \tau_{ij}]) + H(t - [t_A + \tau_{ij} + n\Delta]))$, where $H(t)$ is the Heaviside step function. The instant at which the energy offsets change from ν_i to zero determines the phase φ_{ij} of the effective coupling. For $\tau_{ij} = \frac{\varphi_{ij}}{2(\nu_i - \nu_j)}$ one obtains $\int_{t_A}^{t_B} e^{i2[\chi_i(t') - \chi_j(t')]} dt = e^{i\varphi_{ij} n \Delta}$, where φ_{ij} takes values between zero and 2π . In Fig. 5, the time intervals for tuning the NNN interactions J_2 (intervals I and II) and for tuning NN interactions J_1 (intervals III-VI) have different length [52]. By setting the energy offsets of the atoms to zero during time windows of length n and m respectively, one obtains $\frac{J_2}{J_1} = \frac{n}{m} \cdot \frac{J_2}{J_1}$.

Implementation using nano-photonic systems

Cold atoms trapped near one-dimensional photonics crystals as described in [20, 21] are a very promising platform for realizing strong and tuneable long-range interactions for a large number of atoms. The spin states $|g\rangle$ and $|s\rangle$ can be encoded in ground states of atoms with a lambda configuration, where the excited state is adiabatically eliminated (see Fig. 5b). The photonic modes in the crystal mediate an effective atom-atom interaction of the type given in Eq. (3), with exponentially decaying coupling strength $\bar{J}_{ij} = \bar{J}_0 e^{-\frac{2|r_i - r_j|}{L}}$, where $r_{i/j}$ are the positions of the atoms with indices i, j , and L is the characteristic length of the interaction. The range of the coupling L is tunable through a variation of the system parameters (see [20] for details). The ratio of the parameters n and m in Fig. 5a takes here the value $\frac{n}{m} = e^{\frac{2a}{L}}$, where a is the atomic spacing. Undesired terms with $|i - j| > 2$ are suppressed by a factor $e^{-\frac{4a}{L}}$ or more [53].

Losses

The system is subject to losses which limit the coherence time. The two main loss channels are the spontaneous emission of the atoms into free space and the loss of photons due to imperfections of the photonic crystal. As described in [20], the atoms coupling to light modes in the crystal can be treated in analogy to a cavity QED system with cavity length L . For optimised detuning of the classical driving field, the ratio of the coherent interaction rate \bar{J}_0 to the rate at which the system loses

excitations Γ is determined by the cooperativity C ,

$$\frac{\bar{J}_0}{\Gamma} = \sqrt{C}. \quad (6)$$

The cooperativity depends on the characteristic length L , $C = \frac{L}{\lambda} C_\lambda$, where λ is the resonant wavelength of the atomic transition ($\lambda = 2\pi c/\omega_{ge}$, see Fig. 5b). Depending on the quality factor Q of the photonics crystal, C_λ can take values up to $C_\lambda = 10^4$ (for $Q = 10^6$) or $C_\lambda = 10^5$ (for $Q = 10^7$). For example, a configuration with a distance $a = \frac{3}{2}\lambda$ between the atoms and $L = \frac{3}{\ln(3)}\lambda$ can be implemented with $n = 3$, $m = 1$. This yields an effective cooperativity of $C_{\text{eff}} = 80$ for $Q = 10^7$, where we used $\sqrt{C_{\text{eff}}} = J_0/\Gamma = \sqrt{C} \frac{1}{3(n+2m+2)}$. Hence it should be possible to implement predominantly coherent effective interactions in a system consisting of $\mathcal{O}(10^2)$ atoms.

Required energy scales

In the following, we discuss briefly the required parameter regimes. The time averaged description in Eq. (4) is valid for $\frac{1}{T} \gg (\bar{J}_0, h)$. Therefore the condition

$$v_0 \gg 6\pi(n + 2m + 2) (\bar{J}_0, h)$$

must be fulfilled. Moreover, the shaking procedure must be compatible with the conditions under which the interaction Hamiltonian given in Eq. (3) is valid. As described in [20], this Hamiltonian is obtained by eliminating the light field in the photonics crystal and the excited state $|e\rangle$. In order to prevent real excitations of the photon field mediating the interactions and in order to avoid the population of the excited atomic states, the maximum energy offset in the shaking protocol has to be small compared to the detuning δ_L of the applied classical laser field with respect to the atomic transition (see Fig. 5(b), $\delta_L \gg 4\nu_0$). Finally, the effective couplings have to be large compared to the decoherence rate $\bar{J}_{ij} \gg t_{\text{dec}}^{-1}$. For the following estimate, we assume the decoherence time to be limited by the loss rate Γ discussed above. In summary, we require

$$\begin{aligned} \frac{\delta_L}{4} &\gg v_0 \gg 6\pi(n + 2m + 2) (\bar{J}_0, h) \\ &\gg \frac{18\pi(n + 2m + 2)^2}{t_{\text{dec}}} \sim \frac{18\pi(n + 2m + 2)^2}{\sqrt{C}} \bar{J}_0. \end{aligned} \quad (7)$$

The bare coupling parameter \bar{J}_0 can be approximated by [54]

$$\bar{J}_0 \approx \frac{|\Omega|^2}{\delta_L^2} \sqrt{C} \gamma,$$

where Ω is the Rabi frequency of the applied laser field and γ is the atomic line width (for Cesium atoms $\gamma/(2\pi) \sim 5\text{MHz}$). Using $a = \frac{3}{2}\lambda$ and $L = \frac{3}{\ln(3)}\lambda$, as above ($n = 3$, $m = 1$), we find that the conditions in Eq. (7) can be fulfilled for a sufficiently large detuning δ_L . This

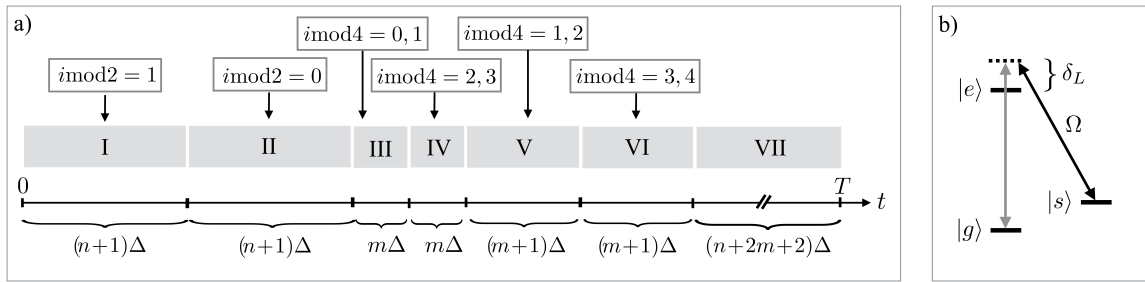


FIG. 5: Realization of artificial gauge fields. (a) Illustration of the protocol described in Sec. . The equations in the grey boxes indicate the positions of the atoms whose energy offset is set to zero during the time intervals I-VI. The full expression for the shaking functions $v_i(t)$ is given in Table II in the main text. (b) Atomic level scheme. A classical field with Rabi frequency Ω couples the states $|s\rangle$ and $|e\rangle$ with detuning δ_L . The states $|g\rangle$ and $|e\rangle$ are coupled via light modes in a photonic crystal.

estimate suggests that the protocol could be realized in principle in its basic form described above. By optimizing the scheme, an enhanced performance and increased robustness can be achieved.

-
- [1] D. R. Hofstadter, Phys. Rev. B **14**, 2239 (1976).
[2] D. Jaksch and P. Zoller, New J. Phys. **5**, 56 (2003).
[3] K. Osterloh *et al.*, Phys. Rev. Lett. **95**, 010403 (2005).
[4] I. I. Satija, D. C. Dakin, J. Y. Vaishnav, and C. W. Clark, Phys. Rev. A **77**, 043410 (2008).
[5] Y.-J. Lin *et al.*, Phys. Rev. Lett. **102**, 130401 (2009).
[6] K. Jiménez-García *et al.*, Phys. Rev. Lett. **108**, 225303 (2012).
[7] S. Powell, R. Barnett, R. Sensarma, and S. Das Sarma, Phys. Rev. Lett. **104**, 255303 (2010).
[8] N. Goldman *et al.*, Phys. Rev. Lett. **105**, 255302 (2010).
[9] M. Burrello and A. Trombettoni, Phys. Rev. Lett. **105**, 125304 (2010).
[10] P. Hauke *et al.*, Phys. Rev. Lett. **109**, 145301 (2012).
[11] J. Struck *et al.*, Phys. Rev. Lett. **108**, 225304 (2012).
[12] M. Aidelsburger *et al.*, Phys. Rev. Lett. **111**, 185301 (2013).
[13] H. Miyake *et al.*, Phys. Rev. Lett. **111**, 185302 (2013).
[14] A. Celi *et al.*, Phys. Rev. Lett. **112**, 043001 (2014).
[15] T. Graß, B. Juliá-Díaz, and M. Lewenstein, Phys. Rev. A **89**, 013623 (2014).
[16] J. Dalibard, F. Gerbier, G. Juzeliūnas, and P. Öhberg, Rev. Mod. Phys. **83**, 1523 (2011).
[17] N. Goldman, G. Juzelinis, P. Öhberg, and I. B. Spielman, Reports on Progress in Physics **77**, 126401 (2014).
[18] D. Porras and J. I. Cirac, Phys. Rev. Lett. **92**, 207901 (2004).
[19] R. Blatt and C. F. Roos, Nat. Phys. **8**, 277 (2012).
[20] J. S. Douglas *et al.*, arXiv 1312.2435 (2013).
[21] A. Goban *et al.*, Nat. Commun. **5**, (2014).
[22] E. Vetsch *et al.*, Phys. Rev. Lett. **104**, 203603 (2010).
[23] A. Goban *et al.*, Phys. Rev. Lett. **109**, 033603 (2012).
[24] Y. Kraus *et al.*, Phys. Rev. Lett. **109**, 106402 (2012).
[25] L.-J. Lang, X. Cai, and S. Chen, Phys. Rev. Lett. **108**, 220401 (2012).
[26] P. Marra, R. Citro, and C. Ortix, arXiv 1408.4457 (2014).
[27] A. Eckardt, C. Weiss, and M. Holthaus, Phys. Rev. Lett. **95**, 260404 (2005).
[28] A. Eckardt and M. Holthaus, EPL **80**, 50004 (2007).
[29] H. Lignier *et al.*, Phys. Rev. Lett. **99**, 220403 (2007).
[30] E. Kierig *et al.*, Phys. Rev. Lett. **100**, 190405 (2008).
[31] C. Sias *et al.*, Phys. Rev. Lett. **100**, 040404 (2008).
[32] A. Zenesini *et al.*, Phys. Rev. Lett. **102**, 100403 (2009).
[33] A. Hemmerich, Phys. Rev. A **81**, 063626 (2010).
[34] J. Struck *et al.*, Science **333**, 996 (2011).
[35] J. Struck *et al.*, Nat Phys **9**, 738 (2013).
[36] G. Jotzu *et al.*, Nature **515**, 237 (2014).
[37] N. Goldman and J. Dalibard, Phys. Rev. X **4**, 031027 (2014).
[38] S. K. Baur, M. H. Schleier-Smith, and N. R. Cooper, Phys. Rev. A **89**, 051605 (2014).
[39] J. Struck, J. Simonet, and K. Sengstock, Phys. Rev. A **90**, 031601 (2014).
[40] A. Bermudez, T. Schaetz, and D. Porras, Phys. Rev. Lett. **107**, 150501 (2011).
[41] P. G. Harper, Proceedings of the Physical Society. Section A **68**, 874 (1955).
[42] D. J. Thouless, M. Kohmoto, M. P. Nightingale, and M. den Nijs, Phys. Rev. Lett. **49**, 405 (1982).
[43] T. Fukui, Y. Hatsugai, and H. Suzuki, J. Phys. Soc. Jpn. **74**, 1674 (2005).
[44] Q. Niu, D. J. Thouless, and Y.-S. Wu, Phys. Rev. B **31**, 3372 (1985).
[45] I. Dzyaloshinskii, J. Phys. Chem. Solids **4**, 241 (1958).
[46] T. Moriya, Phys. Rev. **120**, 91 (1960).
[47] T. Graß, R. W. Chhajlany, C. A. Muschik, and M. Lewenstein, Phys. Rev. B **90**, 195127 (2014).
[48] M. Chen and C. D. Hu, Phys. Rev. B **84**, 094433 (2011).
[49] F. Grusdt and M. Höning, Phys. Rev. A **90**, 053623 (2014).
[50] Y. Hatsugai and M. Kohmoto, Phys. Rev. B **42**, 8282 (1990).
[51] J. Garcia-Ripoll, P. Zoller, and J. Cirac, Phys. Rev. Lett. **91**, 157901 (2003).
[52] The time intervals III and IV have length $m\Delta$ since the effective couplings that are defined in these sections are real, i.e. $\tau_{ij} = 0$.
[53] An even stronger suppression can be achieved by introducing more time intervals
[54] The coupling parameter \bar{J}_0 is given by $\bar{J}_0 = \frac{|\Omega|^2 \bar{g}_c^2}{2\Delta_L \delta_L^2}$, where \bar{g}_c is the light-atom coupling constant. The pa-

parameter and Δ_L is a detuning (see [20] for details) which has to be optimised in order to guarantee a minimal loss-rate as stated in Eq. (6) yielding $\bar{J}_0 = \frac{|\Omega|^2}{\delta_L^2} \sqrt{C} \gamma$. This

expression is used as an estimate, but the actual optimisation is more complicated since Δ_L plays also a role for tuning the characteristic length L .